Article:
Cunningham, VJ, Ratcliffe, LPD, Blanazs, A et al. (2014) Tuning the critical gelation temperature of thermo-responsive diblock copolymer worm gels. Polymer Chemistry, 5 (21). pp. 6307-6317. ISSN: 1759-9954

https://doi.org/10.1039/c4py00856a

Tuning the Critical Gelation Temperature of Thermo-responsive Diblock Copolymer Worm Gels

Victoria J. Cunningham[1], Liam P. D. Ratcliffe[1], Adam Blanazs[1], Nicholas J. Warren[1], Andrew J. Smith[2], Oleksandr O. Mykhaylyk[1,*] and Steven P. Armes[1,*]

[1]*Department of Chemistry, University of Sheffield, Brook Hill, Sheffield, South Yorkshire, S3 7HF, UK.*

[2]*Diamond Light Source Ltd, Diamond House, Harwell Science and Innovation Campus, Didcot, Oxfordshire, OX11 0DE, UK*

Abstract. Amphiphilic diblock copolymer nano-objects can be readily prepared using reversible addition-fragmentation chain transfer (RAFT) polymerization. For example, poly(glycerol monomethacrylate) (PGMA) chain transfer agents (CTA) can be chain-extended using 2-hydroxypropyl methacrylate (HPMA) via RAFT aqueous dispersion polymerization to form well-defined spheres, worms or vesicles at up to 25% solids. The worm morphology is of particular interest, since multiple inter-worm contacts lead to the formation of soft free-standing gels, which undergo reversible degelation on cooling to sub-ambient temperatures. However, the critical gelation temperature (CGT) for such thermo-responsive gels is $\leq$ 20°C, which is relatively low for certain biomedical applications. In this work, a series of new amphiphilic diblock copolymers are prepared in which the core-forming block comprises a statistical mixture of HPMA and di(ethylene glycol) methyl ether methacrylate (DEGMA), which is a more hydrophilic monomer than HPMA. Statistical copolymerizations proceeded to high conversion and low polydispersities were achieved in all cases (M_w/M_n < 1.20). The resulting PGMA-P(HPMA-*stat*-DEGMA) diblock copolymers undergo polymerization-induced self-assembly at 10% w/w solids to form free-standing worm gels. SAXS studies indicate that reversible (de)gelation occurs below the CGT as a result of a worm-to-sphere transition, with further cooling to 5 °C affording weakly interacting copolymer chains with a mean aggregation number of approximately four. This corresponds to almost molecular dissolution of the copolymer spheres. The CGT can be readily tuned by varying the mean degree of polymerization and the DEGMA content of the core-forming statistical block. For example, a CGT of 31°C was obtained for $PGMA_{59}$-P($HPMA_{91}$-*stat*-$DEGMA_{39}$). This is sufficiently close to physiological temperature (37°C) to suggest that these new copolymer gels may offer biomedical applications as readily-sterilizable scaffolds for mammalian cells, since facile cell harvesting can be achieved after a single thermal cycle.

* Author to whom correspondence should be addressed (s.p.armes@sheffield.ac.uk and o.mykhaylyk@sheffield.ac.uk).

Introduction

Recently, stimulus-responsive polymer gels have become an important area of research, with thermo-,[1-4] pH-,[4,5] redox-[6] and light-responsive[7] examples being reported in the literature. There are two main classes of polymer gels. Chemical gels can be formed by the addition of covalent cross-links between polymer chains to form a permanent network. Physical gels are the result of multiple weak intermolecular interactions (e.g. hydrogen bonding, van der Waals interactions etc.) between polymer chains. If constructed using appropriate stimulus-responsive block copolymers, such gels can often exhibit reversible (de)gelation. [1,8,9] For example, injectable physical hydrogels comprising thermo-responsive triblock copolymers composed of ethylene oxide and propylene oxide (PEO/PPO/PEO)[8] provide various biomedical applications, including minimally-invasive implantation and the incorporation of therapeutic agents.[8]

Over the last seven years, polymerization-induced self-assembly (PISA) has been shown to be a versatile and efficient technique for the synthesis of various amphiphilic diblock copolymer nano-objects, with spherical, worm-like, lamella or vesicular morphologies being produced at relatively high copolymer solids.[10-13] More specifically, Blanazs and co-workers[1,9,13,14] have chain-extended a poly(glycerol monomethacrylate)-based macromolecular chain transfer agent (PGMA macro-CTA) with 2-hydroxypropyl methacrylate (HPMA) using a reversible addition-fragmentation chain transfer (RAFT) aqueous dispersion polymerization formulation. Depending on the relative volume fractions of the hydrophilic PGMA and hydrophobic PHPMA blocks, the resulting copolymers can form well-defined spheres, worm-like micelles or vesicles.

The PGMA-PHPMA worms are of particular interest since they form soft free-standing aqueous gels at 20ºC. On cooling to sub-ambient temperatures, degelation occurs at a certain critical gelation temperature (CGT) that depends on the diblock composition, but appears to be less sensitive to the copolymer concentration.[9] Transmission electron microscopy (TEM) and small-angle X-ray scattering (SAXS) studies indicate that degelation is the result of a worm-to-sphere order-order transition.[13] Under certain conditions, this morphological transition is reversible, with spheres reforming the original worms on returning to 20ºC. These PGMA-PHPMA thermo-responsive worm gels exhibit good biocompatibility,[13] so in principle they may be suitable as convenient matrices for long-term storage and/or proliferation of mammalian cells. However, CGT values below 20 °C can lead to the cells experiencing thermal shock, which is likely to reduce their

long-term viability.[15-20] In order to minimize this problem, the design of next-generation copolymer worm gels with higher CGT values is desirable. One approach is to (partially) replace the PHPMA core-forming block with a more hydrophilic monomer such as di(ethylene glycol) methyl ether methacrylate (DEGMA). It is well-known that DEGMA homopolymer exhibits a lower critical solution temperature of 26 °C.[21,22] Thus introducing this comonomer should lead to worm gels exhibiting higher CGT values compared to those reported by Blanazs et al.[1,9]

In the present study, a series of PGMA-P(HPMA-*stat*-DEGMA) statistical diblock copolymers are prepared via RAFT aqueous dispersion polymerization. As expected, these amphiphilic copolymers also undergo polymerization-induced self-assembly to produce worms that form soft free-standing aqueous gels. The mean degree of polymerization of the core-forming block and its DEGMA content have been systematically varied in order to tune the CGT values of these copolymer gels, which have been characterized using TEM, variable temperature ^{1}H NMR spectroscopy, gel rheology measurements, visible absorption spectroscopy and SAXS.

Experimental

Materials

Glycerol monomethacrylate (GMA) was donated by GEO Specialty Chemicals (Hythe, UK) and used without further purification. 2-Hydroxypropyl methacrylate (HPMA), di(ethylene glycol) methyl ether methacrylate (DEGMA; 95 %), 2-cyano-2-propyl dithiobenzoate (CPDB), 4,4'-azobis(4-cyanopentanoic acid) (ACVA; 99 %), NMR solvents (d_4-methanol and deuterium oxide) and anhydrous ethanol (99 %) were purchased from Sigma-Aldrich UK and used as received. Sodium 2,2-dimethyl 2-silapentane-5-sulfonate (DSS) was purchased from Cambridge Isotope Laboratories, Inc. (USA) and used as received. All solvents were purchased from Fisher Scientific (Loughborough, UK) and used as received. De-ionized water was used for all experiments.

Preparation of $PGMA_{59}$ macro-CTA

CPDB RAFT agent (0.802 g, 3.705 mmol) and GMA (40.531 g, 0.253 mol) were weighed into a 250 ml round-bottomed flask and degassed with nitrogen for 15 minutes. ACVA (0.2025 g, 0.722 mmol; CPDB/ACVA molar ratio = 5.0) was added and degassed for a

further 5 min before the addition of anhydrous ethanol (61 ml), which was deoxygenated separately with nitrogen for 30 min prior to addition to the other reagents. The reaction solution was stirred and degassed for a further 5 min before placing in an oil bath at 70°C. The polymerization was allowed to proceed for 140 min, resulting in a monomer conversion of 78 %, as judged by comparing the integrated vinyl peaks at 5.6 and 6.2 ppm to the composite integral at 3.4-4.4 ppm corresponding to the five pendent GMA protons (C*H*$_2$-C*H*OH-C*H*$_2$OH). Methanol (30 mL) was added to the reaction solution, followed by precipitation into a ten-fold excess of chloroform (1.5 L). This purification process was repeated twice to give a purified PGMA macro-CTA (23.13 g, < 1 % residual GMA monomer). ^{1}H NMR analysis indicated a mean degree of polymerization of 59 for this PGMA macro-CTA as judged by end-group analysis (comparison of the integral at 3.4-4.4 ppm (m, 5H, C*H*$_2$-C*H*OH-C*H*$_2$OH) with that assigned to the aromatic RAFT chain-end at 7.4-8.0 ppm (m, 5H, Ph). DMF GPC analysis gave M_n = 16,000 g mol^{-1} and M_w/M_n = 1.18 (against a series of near-monodisperse poly(methyl methacrylate) calibration standards).

Synthesis of PGMA-P(HPMA-*stat*-DEGMA) via RAFT aqueous dispersion polymerization

A typical protocol for the synthesis of a PGMA$_{59}$-P(DEGMA$_{30}$-*stat*-HPMA$_{120}$) diblock copolymer was as follows: PGMA$_{59}$ macro-CTA (0.20 g), DEGMA (0.12 g, 0.653 mmol) and HPMA (0.36 g, 2.48 mmol) were weighed into a 25 ml round-bottomed flask and purged with N_2 for 15 min. ACVA (1.90 mg, 7.0 μmol; CTA/ACVA molar ratio = 3.0) was added to the flask and the mixture was degassed for 5 min. Water (6.13 ml, 10% w/w) which had been degassed separately for 30 min, was added and degassed for a further 10 min, prior to immersion in an oil bath set at 70°C for 16 h. The resulting copolymer was analyzed by DMF GPC (M_n = 41,700 g mol^{-1}, M_w/M_n = 1.14 (against a series of poly(methyl methacrylate) calibration standards).

Characterization

^{1}H NMR Spectroscopy. All ^{1}H NMR spectra were recorded on a 400 MHz Bruker Avance 400 spectrometer using either d_4-methanol or deuterium oxide. For the variable temperature studies, a water suppression programme was utilized to reduce the broad

HDO peak at 4.7 ppm and sodium 2,2-dimethyl 2-silapentane-5-sulfonate was used as an internal standard.

Gel Permeation Chromatography (GPC). The molecular weights and polydispersities of the PGMA macro-CTA, PDEGMA and various diblock copolymers were determined by DMF GPC at 60°C. The GPC set-up consisted of two Polymer Laboratories PL gel 5 μm Mixed C columns connected in series to a Varian 390 LC multi-detector suite (refractive index detector) and a Varian 290 LC pump injection module. The mobile phase was HPLC-grade DMF containing 10 mmol LiBr at a flow rate of 1.0 ml min^{-1}. Copolymer solutions (1.0 w/v %) were prepared using DMF as the solvent and DMSO as the flow rate marker. Ten near-monodisperse poly(methyl methacrylate) standards (PMMA; M_n = 625 – 618,000 g mol^{-1}) were used for calibration. Data were analyzed using Varian Cirrus GPC software (version 3.3).

Dynamic light scattering (DLS). Intensity-average hydrodynamic diameters for the block copolymer nanoparticles were calculated from diffusion coefficients via the Stokes-Einstein equation using a Malvern Zetasizer NanoZS instrument at 20 °C. Light scattering was detected at 173º for 0.20 % w/w aqueous dispersions (unless otherwise stated) using disposable plastic cuvettes and all results were averaged over three consecutive runs. In all cases sphere-equivalent diameters are reported. This is a reasonable approximation for the pseudo-spherical nanoparticles obtained at lower temperatures, but gives only a rather crude indication of the worm dimensions.

Visible absorption spectroscopy. Spectra were recorded between 400 and 800 nm at 37 °C for 10 wt % copolymer dispersions using a Varian Cary 300 Bio UV-visible spectrometer.

Transmission electron microscopy (TEM). Copper/palladium TEM grids (Agar Scientific) were coated in-house to yield a thin film of amorphous carbon. The grids were then subjected to a glow discharge for 30 seconds to create a hydrophilic surface. Individual samples (0.2 w/v % aqueous dispersion, 10.0 μL) were adsorbed onto the freshly treated grids for 1.0 min and then blotted with filter paper to remove excess solution. To stain the colloidal aggregates, uranyl formate (9.0 μL of a 0.75 w/v % solution) was absorbed onto the sample-loaded grid for 20 seconds and then carefully blotted to remove excess stain.

The grids were then dried using a vacuum hose. Imaging was performed using a Phillips CM100 instrument operating at 100 kV and equipped with a Gatan 1 k CCD camera.

Rheology. Critical gelation temperatures were determined using an AR-G2 rheometer (TA Instruments). A variable temperature Peltier plate was used in conjunction with a 40 mm 2° aluminium cone. Temperature sweeps were conducted at a fixed strain value (1.0 %) and at an angular frequency of 10 rad s^{-1}. Storage (G') and loss (G'') moduli were monitored and the critical gelation temperature was calculated from the cross-over of these two curves.

Small angle X-ray scattering (SAXS). SAXS patterns were collected at a synchrotron source (Diamond Light Source, station I22, Didcot, United Kingdom) using monochromatic X-ray radiation (wavelength λ = 0.10 nm, camera length = 9.4 m, covering a q range from 0.02 nm^{-1} to 1.7 nm^{-1}, where $q = \frac{4\pi \sin\theta}{\lambda}$ is the length of the scattering vector and θ is half of the scattering angle) and a 2D Pilatus 2M CCD detector. A liquid cell comprising two mica windows (each of 25 μm thickness) separated by a polytetrafluoroethylene spacer of 1 mm thickness was used as a sample holder. The body of the cell was connected to a water bath to perform SAXS measurements during cooling and heating ramps (from 40°C to 5°C and from 5°C to 40°C at a rate of 1 °C per min). Time-resolved SAXS patterns were recorded at a rate of 1 frame per min using a frame acquisition time of 1 second. The thermocouple controlling the sample temperature was inserted directly into the aqueous dispersion. Scattering data reduced by Nika SAS data reduction macros for Igor Pro (integration, normalization, background subtraction) were further analyzed using Irena SAS macros for Igor Pro[23]. Glassy carbon was used for absolute intensity calibration.[24] Measurements were conducted on an aqueous dispersion of $PGMA_{59}$-($PDEGMA_{39}$-*stat*-$PHPMA_{91}$) (mass fraction = 0.048 as measured using a moisture analyzer). Since these diblock copolymer dispersions are temperature-sensitive[1], the liquid cell was shifted to a new position for each time frame during data acquisition to prevent the X-ray beam causing local heating of the sample.

Results and Discussion

A low polydispersity $PGMA_{59}$ macro-CTA (M_w/M_n = 1.18) was prepared in ethanol at 70°C by RAFT solution polymerization. The crude PGMA macro-CTA was purified by precipitation into excess chloroform. ^{1}H NMR spectroscopy indicated a mean degree of polymerization (DP) of 59 for this PGMA macro-CTA. This macro-CTA was then utilized for the RAFT aqueous dispersion polymerization of DEGMA, where the target DP of the core-forming block was systematically varied from 100 to 400 (see Table S1 in the Supporting Information). According to ^{1}H NMR analysis, all polymerizations proceeded to at least 97 % conversion, with more than 99 % conversion being achieved in many cases.

DMF GPC analysis of these $PGMA_{59}$-$PDEGMA_x$ diblock copolymers indicated high blocking efficiencies with minimal $PGMA_{59}$ macro-CTA contamination. However, significantly higher polydispersities (M_w/M_n >> 1.20) were obtained when targeting higher DPs for the PDEGMA block. Similar observations have been attributed to dimethacrylate contamination of the core-forming monomer.[13] Thus column chromatography (using a silica stationary phase) was utilized to remove dimethylacrylate impurities from the DEGMA monomer. This purification protocol led to a substantial reduction in the polydispersity of the $PGMA_{59}$-$PDEGMA_x$ diblock copolymer (see Figure S1). Unfortunately, no $PGMA_{59}$-$PDEGMA_x$ gels were formed despite removing the dimethacrylate impurity. Given the well-known thermo-responsive nature of PDEGMA,[22,25,26] this negative result was wholly unexpected.

As an alternative approach, it was envisaged that a core-forming block consisting of a *statistical* P($HPMA_x$-$DEGMA_y$) copolymer might provide the desired thermo-responsive worm gels with higher CGT values relative to the prototypical PGMA-PHPMA formulation (see Scheme 1).[1,9] Accordingly, a range of $PGMA_{59}$-P($HPMA_x$-$DEGMA_y$) statistical diblock copolymers were synthesized with an overall target DP (x + y) for the core-forming block ranging from 140 to 160 and a DEGMA content of 10, 20 or 30 mol%.

All $PGMA_{59}$-P($HPMA_x$-*stat*-$DEGMA_y$) statistical diblock copolymer syntheses proceeded to high conversions as judged by ^{1}H NMR spectroscopy, while DMF GPC studies confirmed that high blocking efficiencies were obtained (see Table 1 and Figure 1). A linear evolution in number-average molecular weight (M_n) with conversion was observed and low polydispersities (M_w/M_n < 1.20) were achieved for all copolymers,

indicating that good RAFT control was maintained during aqueous dispersion copolymerization. All $PGMA_{59}$-P(HPMA-*stat*-DEGMA) diblock copolymers were prepared using the unpurified DEGMA monomer: given their relatively low DEGMA contents, the dimethacrylate impurity has relatively little effect on the copolymer molecular weight distribution as judged by DMF GPC analysis. The resulting copolymer dispersions formed free-standing worm gels at 10% w/w solids, which could be reversibly switched to a free-flowing liquid on lowering the solution temperature. During statistical copolymerization at 70°C, a free-flowing dispersion was obtained which has been previously observed by Blanazs and co-workers [1,9] for PGMA-PHPMA worms. This is because these worm gels exhibit shear-thinning behaviour: no gelation occurs provided that the reaction mixture is continually stirred. On cooling, $PGMA_{59}$-P($HPMA_{144}$-*stat*-$DEGMA_{16}$) and $PGMA_{59}$-P($HPMA_{128}$-*stat*-$DEGMA_{32}$) formed soft-free standing gels at 20°C on cessation of stirring, whereas all other statistical diblock copolymers formed either viscous liquids or free-flowing liquids. However, heating these copolymer dispersions to above ambient temperature led to the formation of soft free-standing gels in each case.

Rheology

Gel rheology studies were performed to determine the CGT for each copolymer dispersion. The storage (G') and loss moduli (G'') were monitored against temperature and the CGT was determined by the point of intersection of these two curves. Figure 2a shows the rheological data obtained for $PGMA_{59}$-P($HPMA_{144}$-*stat*-$DEGMA_{16}$) and $PGMA_{59}$-P($HPMA_{126}$-*stat*-$DEGMA_{14}$) on heating from 10°C to 40°C in 1°C increments. The CGTs for these two copolymers were determined to be 16°C and 23°C, respectively. A monotonic reduction in the CGT was observed as the DP of the core-forming block was increased for $PGMA_{59}$-P(HPMA-*stat*-DEGMA) copolymers containing either 10, 20 or 30 mol % DEGMA (see Figure 2b). Longer copolymer chains required a greater degree of hydration of the core-forming block to induce the worm-to-sphere transition, which necessitates accessing a lower temperature.[27] Increasing the DEGMA content leads to a higher CGT because the DEGMA repeat unit is more hydrophilic than the HPMA repeat unit (DEGMA monomer is water-miscible in all proportions, whereas HPMA monomer is only water-miscible up to 13% at 20°C). In principle, this approach should enable specific CGT values to be targeted. Higher CGTs can also be achieved by targeting copolymers with shorter core-forming blocks (Figure 3). For example, $PGMA_{59}$-P($HPMA_{77}$-*stat*-

DEGMA$_{36}$), PGMA$_{59}$-P(HPMA$_{84}$-*stat*-DEGMA$_{36}$) and PGMA$_{59}$-P(HPMA$_{91}$-*stat*-DEGMA$_{39}$) each exhibit CGT values above 30°C, which should be sufficiently high to minimize thermal shock if these gels were to be used as cell growth media[15-20] or related biomedical applications. Digital photographs recorded for PGMA$_{59}$-P(HPMA$_{91}$-*stat*-DEGMA$_{39}$) at 20°C and 40°C (see inset, Figure 3) show that a relatively transparent free-flowing pink liquid is observed at 20°C, suggesting the presence of spherical nanoparticles, rather than worms. As this statistical block copolymer is heated, these spherical particles self-assemble to form worm-like micelles which interact to produce a turbid pale pink gel above a CGT of 31°C; this is confirmed by the presence of worm-like micelles by TEM (Figure 4). Serial dilution of this copolymer dispersion combined with the tube inversion test indicated a critical gelation concentration (CGC) of ~ 3.5% w/w, which is comparable to that reported for the PGMA-PHPMA diblock copolymers prepared by Verber et al.[9]

Turbidimetry

The turbidity of three PGMA$_{59}$-P(HPMA$_x$-*stat*-DEGMA$_y$) copolymer gels (and also an aqueous solution of the corresponding PGMA$_{59}$ macro-CTA) was assessed at 10% w/w solids at 37°C. Figure 5a shows the date obtained for these three copolymers, which were prepared with differing DEGMA contents but the same fixed overall target DP for the core-forming block. In general, incorporation of more DEGMA comonomer leads to more turbid gels. For example, the PGMA$_{59}$-P(HPMA$_{144}$-*stat*-DEGMA$_{16}$) gel is significantly less turbid at 37 °C than the PGMA$_{59}$-P(HPMA$_{112}$-DEGMA$_{48}$) gel. Figure 5b shows the variation of core-forming block DP on the turbidity of the copolymer gels. A relatively short core-forming block DP leads to more transparent gels, with PGMA$_{59}$-P(HPMA$_{98}$-DEGMA$_{42}$) being only slightly more turbid than the molecularly dissolved PGMA$_{59}$ macro-CTA at 10% w/w solids (see Figure 5b).

Figure 5c shows the change in absorbance in the visible region recorded for a 10% w/w PGMA$_{59}$-P(HPMA$_{91}$-DEGMA$_{39}$) aqueous dispersion during a 40°C - 25°C - 5°C - 25°C - 40°C temperature cycle. Reduced turbidity is observed on lowering the temperature. This provides further evidence for the worm-to-sphere transition, since the smaller spheres scatter less light than the worms; this change in morphology reduces the absorbance, particularly at shorter wavelengths. Moreover, this change in turbidity exhibits excellent reversibility on returning to 40°C. This is consistent with the

rheological data obtained for these thermo-responsive gels and suggests that the original worm phase is reformed at this temperature.

Variable temperature ^{1}H NMR studies

The extent of hydration of the statistical core-forming block for PGMA$_{59}$-P(HPMA$_{91}$-*stat*-DEGMA$_{39}$) was assessed by variable temperature ^{1}H NMR spectroscopy in D_2O. It has been previously reported that both PHPMA and PDEGMA blocks become more hydrated at lower temperatures.[1,28] This is also observed in the ^{1}H NMR spectra recorded for PGMA$_{59}$-P(HPMA$_{91}$-*stat*-DEGMA$_{39}$), see Figure 6. A pendent methyl signal (h) assigned to the HPMA residues is highlighted. Its intensity gradually decreases on warming from 5 °C to 20°C, and all but disappears above 25 °C. This suggests that the PHPMA chains are more hydrated at sub-ambient temperatures, which is consistent with the thermo-sensitive behavior of these copolymer gels.[1,9] Similar behavior is observed for the pendent methyl protons assigned to the DEGMA component of this statistical diblock copolymer. The core-forming block is relatively well-hydrated at 5-20 °C, resulting in prominent signals at 0.95 ppm and 3.12 ppm. However, these signals become progressively attenuated above 20°C, suggesting that the core-forming block is less solvated and/or has reduced mobility. Variable temperature DLS studies of a 0.20% w/w dispersion of PGMA$_{59}$-P(HPMA$_{91}$-*stat*-DEGMA$_{39}$) show a morphological transition at 23°C from unimers (< 10 nm) to spheres with a z-average hydrodynamic diameter of ~ 30 nm. This transition coincides with the spectral changes that are observed between 20 ºC and 25 ºC. From 25 ºC to 40 °C a further modest reduction in chain hydration is observed. DLS studies do not provide any evidence for a sphere-to-worm transition, but it is noted that worm formation is unlikely to occur on normal experimental time scales (hours/days) at the relatively low copolymer concentration (0.20% w/w) required for this light scattering technique.[9]

SAXS studies

A 40 ºC – 25 ºC – 5 ºC – 25 ºC – 40 ºC temperature cycle was conducted on a 4.8% w/w aqueous dispersion of PGMA$_{59}$-P(HPMA$_{91}$-*stat*-DEGMA$_{39}$). There is a continuous evolution in the SAXS pattern during cooling (see Figure 7) and heating (data not shown). Significant reductions in the X-ray scattering intensity at low q are discernible at both 30°C and 10°C (see arrows in Figure 7), which suggests two thermally-induced morphological transitions. Three distinctive SAXS patterns can be identified in the time-

resolved measurements (Figure 8): one at approximately 40°C, another in the middle of the cycle (at around 20ºC) and a third at 5°C. Taking into account the TEM observations (see Figure 4) and the previously reported SAXS data obtained for a closely related $PGMA_{54}$-$PHPMA_{140}$ formulation,[1] the first two patterns correspond to worm-like and spherical micelles, respectively. At first sight, the third pattern suggested molecularly-dissolved copolymer chains. Thus three structural models were selected to analyze these SAXS patterns: worm-like micelles[29,30], spherical micelles[29,31] and a generalized Gaussian coil for polymer solutions[32].

In general, the X-ray intensity scattered by a dispersion of nano-objects (usually represented by the scattering length density per unit sample volume, $d\Sigma/d\Omega$ (q)) can be expressed as a product of their form factor, $F(q)$, the structure factor, $S(q)$, and the volume fraction ϕ, divided by the volume of the nano-object, V_{obj}, as shown below.

$$\frac{d\Sigma}{d\Omega}(q) = \frac{\phi}{V_{obj}} F(q)S(q) \qquad (1)$$

The worm-like particles can be described as semi-flexible chains with a circular cross-section, hence the form factor for such anisotropic nano-objects can be expressed as[29]

$$F_{w\_mic}(q) = N_w^2 \beta_s^2 F_{sw}(q) + N_w \beta_c^2 F_c(q, R_g) + N_w (N_w - 1)\beta_c^2 S_{cc}(q) + 2N_w^2 \beta_s \beta_c S_{sc}(q) \qquad (2)$$

where the core block and the corona block X-ray scattering length contrast is given by $\beta_s = V_s(\xi_s - \xi_{sol})$ and $\beta_c = V_c(\xi_c - \xi_{sol})$, respectively. Here ξ_s, ξ_c, and ξ_{sol} are the X-ray scattering lengths of the core block [$\xi_{PHPMA91\text{-}stat\text{-}PDEGMA39}$ = (11.11 × 91 + 10.61 × 39)/130 × 10^{-10} cm^{-2} = 10.92 × 10^{10} cm^{-2}], the corona block (ξ_{PGMA} = 11.94 × 10^{10} cm^{-2}) and the solvent (ξ_{H2O} = 9.42 × 10^{10} cm^{-2}), respectively. V_s and V_c are volumes of the core block ($V_{PHPMA91\text{-}stat\text{-}PDEGMA39}$ = 18.0 nm^3 + 10.6 nm^3 = 28.6 nm^3) and the corona block (V_{PGMA59} = 12.0 nm^3), respectively. The volumes were obtained from $V = \frac{M_w}{N_A \rho}$ using solid-state homopolymer densities determined by helium pycnometry (ρ_{PHPMA} = 1.21 g cm^{-3}, ρ_{PDEGMA} = 1.15 g cm^{-3} and ρ_{PGMA} = 1.31 g cm^{-3},). The self-correlation term for the worm micelle core with radius R_{sw}, $F_{sw}(q) = F_{worm}(q, L_w, b_w)A^2_{cs\_worm}(q, R_{sw})$, is a product of a core cross-

section term $F_{cs\_worm}(q,R_{sw}) = A^2_{cs\_worm}(q,R_{sw}) = \left[2\frac{J_1(qR_{sw})}{qR_{sw}}\right]^2$, where J_1 is the first-order Bessel function of the first kind, and a form factor for self-avoiding semi-flexible chains representing the worm $F_{worm}(q, L_w, b_w)$, where b_w is the worm Kuhn length and L_w is the mean worm contour length. A complete expression for the chain form factor can be found elsewhere[30] (Eq. 26 of this reference with the formalism described therein was used in the present work). The self-correlation term of the corona block in Eq. (2) is given by the Debye function $F_c(q,R_g) = \frac{2[\exp(-q^2R_g^2) - 1 + q^2R_g^2]}{q^4R_g^4}$. The interference cross-term between the worm-like micelle core and the coronal stabilizer chains is taken to be: $S_{sc}(q) = \psi(qR_g)A_{cs\_worm}J_0[q(R_{sw}+R_g)]F_{worm}(q,L_w,b_w)$, where $\psi(qR_g) = \frac{1-\exp(-q^2R_g^2)}{q^2R_g^2}$ is the form factor amplitude of the corona chain, R_g is the radius of gyration of the corona block (PGMA), and J_0 is the zero-order Bessel function of the first kind. The interference term between the worm corona chains is taken to be:

$$S_{cc}(q) = \psi^2(qR_g)J_0^2[q(R_{sw}+R_g)]F_{worm}(q,L_w,b_w)$$

The mean aggregation number of the worm-like micelles is $N_w = (1-x_{sol})\frac{\pi R_{sw}^2 L}{V_s}$, where x_{sol} is the solvent volume fraction within the worm micelle core. Possible hemi-spherical caps at each end of the worms[33] are not included in the form factor model, Eq. (2). It is usually accepted[34] that $S(q) = 1$ for sufficiently low nanoparticle concentrations (typically a few volume percent). For higher concentrations, a structure factor based on the polymer reference interaction site model (PRISM) proposed for interacting worm-like micelles can be used:[35]

$$S_w(q) = \frac{1}{1+\mu(\phi)F_{rod}(q,L_c)F_{worm}(q,L_w,b_w)} \quad (3)$$

where $\mu(\phi)$ is an effective coefficient depending on the nanoparticle volume fraction, $F_{rod}(q,L_c)$ is the form factor of an infinitely thin rod[29] and L_c denotes a characteristic length.

The spherical micelle form factor used in Eq. (1) is given by:[29]

$$F_{s\_mic}(q) = N_s^2 \beta_s^2 A_s^2(q, R_s) + N_s \beta_c^2 F_c(q, R_g) + N_s(N_s - 1)\beta_c^2 A_c^2(q) + 2N_s^2 \beta_s \beta_c A_s(q, R_s) A_c(q) \quad (4)$$

If not stated otherwise, parameters and functions in this model are analogous to the worm-like micelle model, Eq. (2). The sphere form factor amplitude is used for the amplitude of the core self-term, $A_s(q, R_s) = \frac{3[\sin(qR_s) - qR_s \cos(qR_s)]}{(qR_s)^3}$, where R_s is the radius of the spherical micelle core. The form factor amplitude of the spherical micelle corona is $A_c(q) = \psi(qR_g)\frac{\sin[q(R_s + R_g)]}{q(R_s + R_g)}$. The aggregation number of the spherical micelle is $N_s = (1 - x_{sol})\frac{4\pi R_s^3}{3V_s}$. An effective structure factor expression proposed for interacting spherical micelles[34] has been used in Eq. (1):

$$S_s(q) = 1 + \frac{A_{s\_mic}^{av}(q)^2 [S_{PY}(q, R_{PY}, f_{PY}) - 1]}{F_{s\_mic}(q)} \quad (5)$$

Herein the form factor of the average radial scattering length density distribution function of micelles is used as $A_{s\_mic}^{av}(q) = N_s[\beta_s A_s(q, R_s) + \beta_c A_c(q)]$ and $S_{PY}(q, R_{PY}, f_{PY})$ is a hard-sphere interaction structure factor based on the Percus-Yevick approximation[36], where R_{PY} is the interaction radius and f_{PY} is the hard-sphere volume fraction. A sharp interface (i.e. no sigmoidal interface) between the two blocks was assumed for both micelle form factors, Eq. (2) and Eq. (4). In addition, it is assumed that there is no penetration of the coronal stabilizer chains within the micelle cores.

The experimental SAXS pattern obtained for the original diblock copolymer worms at 40°C can be satisfactorily fitted using the worm-like model, Eq. (2), assuming that $S_w(q)$ = 1 (Figure 8). Moreover, the calculated micelle core cross-section (17.4 nm) and the mean worm contour length (102 nm) (Table 2) are consistent with the TEM images (Figure 4). The experimental R_g for the corona PGMA block (1.8 nm) is also physically reasonable, since this parameter can be estimated as follows. The projected contour length of a GMA repeat unit is 0.255 nm (two C-C bonds in *all-trans* conformation), the total contour length of a $PGMA_{59}$ block, L_{PGMA} = 59 × 0.255 nm = 15.05 nm. Given a mean Kuhn

length of 1.53 nm [based on the known literature value for PMMA[37]] indicates an unperturbed radius of gyration, $R_g = (15.05 \times 1.53/6)^{0.5}$, or 1.96 nm. More importantly, the copolymer volume fraction of 0.036 obtained from SAXS analysis (Table 2) corresponds to a mass fraction of 0.044, which is consistent with the experimental mass fraction of 0.048 (or 4.8% solids). Given this relatively high copolymer concentration, a slightly underestimated volume fraction from the SAXS model fitting could be the result of the worm-like micelle interaction reducing the scattered X-ray intensity at low q.[35] Unfortunately, there was no opportunity to determine the effect of copolymer concentration on the scattering profile in the present SAXS study, hence $\mu(\phi)$ cannot be evaluated for Eq. (3). However, assuming $\mu(\phi) = 0.05$ and including the structure factor given by Eq. (3) in the fitting model, similar parameters were calculated (Table 2). L_c was determined as described in an earlier study.[35] In summary, the worm-like micelle model describes the morphology of the PGMA$_{59}$-P(HPMA$_{91}$-*stat*-DEGMA$_{39}$) nano-objects reasonably well.

In contrast, the best fits to SAXS patterns recorded for the same copolymer dispersion at intermediate temperatures (e.g. 20 °C) are obtained using the spherical micelle model described by Eq. (4) and Eq. (5) (see Figure 8). This finding supports previous observations made for a closely-related PGMA$_{54}$-PHPMA$_{140}$ formulation:[1] the worm-like PGMA$_{59}$-P(HPMA$_{91}$-*stat*-DEGMA$_{39}$) micelles transform into spherical micelles upon cooling, because the greater hydration of the core-forming block leads to a subtle reduction in the packing parameter.[38] Since the corona contribution to the scattering signal is comparable to the scattering from the core [$(\beta_c / \beta_s)^2 \approx 0.50$], a rigorous corona scattering length density radial profile represented by a linear combination of two cubic b spline functions[31] (with two fitting parameters s and a corresponding to the width of the profile and the functions weight coefficient, respectively) was also evaluated for SAXS data fitting to a spherical micelle model. This rigorous model produces the corona profile fitting parameters s = 4.7 nm and a = 0.10, which yields comparable results to those obtained using the model based on the polymer chain form factor amplitude $\psi(qR_g)$, Eq. (4), (Table 2). This suggests that $\psi(qR_g)$ used for the corona blocks is a good approximation for the PGMA$_{59}$-(PDEGMA$_{39}$-*stat*-PHPMA$_{91}$) micelles. The micelle core diameter (19.2 nm) is comparable to the mean worm width (17.4 nm). Thus the spherical micelles can be considered to be building blocks for the worms. Like the worm-like

micelles, the R_g of the corona block in the spherical micelles (2.3 nm) is close to the calculated value (1.96 nm). Although a good data fit can be obtained, the calculated copolymer volume fraction (0.087) is about twice that of the expected value. Since the aqueous copolymer dispersion was sealed during the temperature ramp experiments, there cannot be any change in copolymer concentration. Moreover, any changes in the X-ray scattering length contrast of the various components should be insignificant within the relatively narrow temperature range used in these experiments. This speculation is supported by the fact that the Porod invariant remains nearly constant ($Q \approx 2 \times 10^{20}$ cm^{-4}) during the temperature cycle (Fig. 8, inset). Thus the overestimated ϕ value obtained from the spherical micelle data fitting suggests that this model does not include all physically meaningful parameters. In principle, this apparent inconsistency can be resolved by assuming that the spherical micelles represent an intermediate morphology and that the copolymer dispersion obtained at intermediate temperatures (~ 20°C) represents a binary mixture of spherical micelles and almost molecularly-dissolved copolymer chains. Nevertheless, this two-component model was not invoked for a more sophisticated SAXS analysis, since the simple spherical micelle model already provides sufficiently high-quality data fits. However, incorporation of the molecularly-dissolved component *would* be required to properly account for the copolymer concentration, which is otherwise too high for a pure sphere population.

Upon cooling to 5 °C the scattered X-ray intensity is significantly reduced at low q (Figure 8). The SAXS pattern is relatively featureless, which is consistent with dissociation of the spherical micelles to afford almost molecularly-dissolved copolymer chains. Similar patterns, albeit at even lower temperatures, have been recently reported for an aqueous dispersion of a $PGMA_{57}$-$PHPMA_{140}$ diblock copolymer.[39] This is reasonable, since incorporation of the relatively hydrophilic DEGMA comonomer should favor molecular dissolution.

The scattered intensity for an individual Gaussian polymer chain can be expressed as

$$\frac{d\Sigma}{d\Omega}(q) = \phi(\Delta\xi)^2 V_{mol} F_{mol}(q) \qquad (6)$$

where $\Delta\xi$ is the excess scattering length density of the copolymer and V_{mol} is the total volume of the molecule. The generalized form factor for a Gaussian polymer chain is given by[32]

$$F_{mol}(q) = \left[\frac{1}{\nu U^{1/(2\nu)}} \gamma\left(\frac{1}{2\nu}, U\right) - \frac{1}{\nu U^{1/\nu}} \gamma\left(\frac{1}{\nu}, U\right) \right] \quad (7)$$

with the modified variable $U = (2\nu+1)(2\nu+2)\frac{q^2 R_g^2}{6}$, where ν is the excluded volume parameter and $\gamma(s,x) = \int_0^x t^{s-1} \exp(-t)dt$ is the lower incomplete gamma function. Thus two fitting parameters are used for $F_{mol}(q)$. Fitting to the 5 °C SAXS pattern yields $\nu = 0.45$ and $R_g = 5.4$ nm (Figure 8).

The ν parameter is close to 0.50, which corresponds to theta solvent conditions. The R_g value is consistent with DLS studies of the same aqueous copolymer dispersion, which reported a mean hydrodynamic radius of 5.9 nm. However, using the known Kuhn length for PMMA (b = 1.53 nm) and the above value for ν, the R_g of a single copolymer chain was estimated to be only 3.1 nm:[32,37]

$$R_g = \frac{b^{2(1-\nu)} L_{mol}^{2\nu}}{(2\nu+1)(2\nu+2)} \quad (8)$$

where L_{mol} = (59 + 91 + 39) × 0.255 nm = 48.2 nm corresponds to the total contour length of the copolymer chain, assuming that each block has the same projected contour length per monomer repeat unit of 0.255 nm (i.e two C-C bonds in an *all-trans* conformation). The difference between the calculated and experimental values (5.4 nm vs. 3.1 nm) suggests that the spherical micelles do not fully dissociate to form individual chains in aqueous solution on cooling to 5 °C. This conclusion was supported by DLS studies of the same diblock copolymer in methanol, which is a good solvent for both blocks and hence ensures true molecular dissolution. This DLS experiment indicated a mean hydrodynamic radius of 3.0 nm, which is comparable to the calculated R_g of 3.1 nm. This confirms that the copolymer is fully dissolved in methanol, but is only partially dissolved in water at 5 °C. The absolute SAXS intensity scale (Figure 8) provides an opportunity for an additional estimation. If the copolymer chains are fully dissolved in water at 5 °C, then the volume of a scattering object should be equal to the volume occupied by an individual copolymer chain, V_{mol} = 40.6 nm for the copolymer studied here. According to Eq. (6) the SAXS intensity at low q ($q \sim 0$ nm^{-1}) should be approximately 0.53 cm^{-1} [$I(0) = 0.04 \times (1.8 \times 10^{10}$ cm$^{-2})^2 \times 40.6$ nm^3, where ϕ = 0.04 corresponds to a 4.8 wt% aqueous copolymer solution and $\Delta\xi = 1.8 \times 10^{10}$ cm^{-2} is the difference between the mean scattering length density of the copolymer, 11.22×10^{10} cm^{-2}, and the scattering length

density of water, 9.42×10^{10} cm^{-2}]. In reality, the experimental SAXS intensity for the 5 °C pattern at low q is approximately 2.3 cm^{-1} (Figure 8), suggesting that the mean volume of the scattering objects is about four times larger than that of the copolymer chains. Assuming that four copolymer chains can be represented by a single molecule with a four-fold higher contour length (i.e. $4L_{mol}$) in Eq. (8), the R_g of this hypothetical molecule should be 5.7 nm, which is quite close to the R_g of 5.4 nm indicated by SAXS. Thus both the absolute X-ray scattering intensity and the radius of gyration calculated from the data fit to the Gaussian polymer chain model [see Eq. (7)] suggest that, on cooling to 5 °C, aqueous dispersions of $PGMA_{59}$-($PDEGMA_{39}$-*stat*-$PHPMA_{91}$) spherical micelles dissociate to form weakly interacting aggregates comprising approximately four copolymer chains. As a comparison, we estimate N_w to be 551 for the worms (at 40 °C) and N_s to be 56 for the spheres (at 20 °C) using the same approach. Finally, given the hydroxy-functional nature of these methacrylic copolymers, it seems likely that hydrogen bonding may play an important role in the formation of these intermolecular aggregates.

Both SAXS and turbidimetry studies indicate that the thermally-induced morphological transformations are fully reversible for these new statistical diblock copolymers. Scattering patterns corresponding to the initial and final temperature (40 °C) of the thermal cycle overlap quite well with each other (Figure 8). Moreover, the structural parameters calculated for the worm-like micelles at 40 °C before cooling and after heating are virtually identical (Table 2). Some minor deviations between SAXS patterns are observed in the middle of the thermal cycle (Figure 8). The structure factor parameters calculated by fitting the SAXS patterns recorded at intermediate temperatures to the spherical micelle model suggest that the micelles at 20 °C are more close-packed during the cooling ramp compared to the heating ramp (the radius of interaction, R_{PY}, is smaller, while the volume fraction, f_{PY}, is higher). However, such behavior is not unexpected: the worm-to-sphere transformation that occurs on *cooling* should initially afford close-packed spheres, whereas the sphere-to-worm transition that occurs on *heating* necessarily involves the sequential co-operative self-assembly of randomly-distributed spheres to form worm-like micelles.

Surface plasticization of worm cores has recently been invoked to account for the worm-to-sphere morphology transition that is observed on *heating* poly(lauryl methacrylate)-

poly(benzyl methacrylate) worms in *n*-dodecane.[40] It seems likely that similar solvent plasticization (i.e. worm core hydration via penetration of water molecules) is also responsible for the worm-to-sphere transition observed on *cooling* an aqueous copolymer worm dispersion in the present study. This hypothesis is fully consistent with the variable temperature ^{1}H NMR observations (see Figure 6) and would be expected to lead to the reduction in the molecular packing parameter for the copolymer chains that is required to induce a worm-to-sphere transition. This interpretation is also in agreement with the SAXS data shown in Table 2, which suggests an increase in the solvent volume fraction in the micelle cores.

Conclusions

New thermo-responsive copolymer worm gels with tunable critical gelation temperatures (CGT) have been synthesized by systematically increasing the DEGMA content of a series of PGMA$_{59}$-P(HPMA$_x$-*stat*-DEGMA$_y$) statistical diblock copolymers. For example, PGMA$_{59}$-P(HPMA$_{77}$-*stat*-DEGMA$_{36}$), PGMA$_{59}$-P(HPMA$_{84}$-*stat*-DEGMA$_{36}$) and PGMA$_{59}$-P(HPMA$_{91}$-*stat*-DEGMA$_{39}$) worm gels exhibit CGT values greater than 30^{o}C, which is sufficiently close to physiological temperatures to minimize thermal shock. Thus such gels may have potential applications as biocompatible matrices for cell growth and/or long-term cell storage. Conversely, increasing the DP of the statistical core-forming block for PGMA$_{59}$-P(HPMA-*stat*-DEGMA)$_x$ worm gels prepared using 30 mol% DEGMA leads to a *reduction* in the CGT from 42 ^{o}C for x = 110 to 21 ^{o}C for x = 160.

The turbidity of PGMA-P(HPMA-*stat*-DEGMA) diblock copolymer worm gels varies significantly, depending on both the DEGMA content and the mean DP of the core-forming block. The most transparent worm gels are obtained when targeting a relatively short core-forming block DP and a low DEGMA content. Variable temperature ^{1}H NMR studies confirm that the core-forming block becomes much more solvated and/or mobile at lower temperature. Detailed SAXS analysis confirms that semi-flexible worm-like micelles exist at 40^{o}C, but are transformed via an order-order transition into spherical micelles on cooling to 20°C. Further cooling to 5°C leads to almost molecularly-dissolved copolymer chains. These two thermal transitions are fully reversible and coincide with a change in the volume fraction of solvent in the micelle core, which is consistent with the variable temperature ^{1}H NMR studies.

Supporting Information Available

Experimental details for the synthesis of PGMA-PDEGMA diblock copolymers. Summary of monomer conversions and GPC data for $PGMA_{59}$-$PDEGMA_x$ and DMF GPC curves for $PGMA_{59}$-$PDEGMA_{400}$ prepared using DEGMA monomer before and after its purification via silica column chromatography. This material is available free of charge via the Internet at http://pubs.acs.org.

Acknowledgments

SPA thanks the European Research Council (ERC) for a five-year *Advanced Investigator* grant (PISA 320372) and EPSRC is also acknowledged for their support of OOM via Platform grant EP/ J007846/1. The Diamond light source is thanked for the allocation of synchrotron beam-time.

References

(1) Blanazs, A.; Verber, R.; Mykhaylyk, O. O.; Ryan, A. J.; Heath, J. Z.; Douglas, C. W. I.; Armes, S. P. *Journal of the American Chemical Society* **2012**, *134*, 9741.

(2) Li, C.; Tang, Y.; Armes, S. P.; Morris, C. J.; Rose, S. F.; Lloyd, A. W.; Lewis, A. L. *Biomacromolecules* **2005**, *6*, 994.

(3) Madsen, J.; Armes, S. P.; Lewis, A. L. *Macromolecules* **2006**, *39*, 7455.

(4) Schilli, C. M.; Zhang, M.; Rizzardo, E.; Thang, S. H.; Chong, Y. K.; Edwards, K.; Karlsson, G.; Müller, A. H. E. *Macromolecules* **2004**, *37*, 7861.

(5) Ma, Y.; Tang, Y.; Billingham, N. C.; Armes, S. P.; Lewis, A. L. *Biomacromolecules* **2003**, *4*, 864.

(6) Li, C.; Madsen, J.; Armes, S. P.; Lewis, A. L. *Angewandte Chemie International Edition* **2006**, *45*, 3510.

(7) Woodcock, J. W.; Wright, R. A.; Jiang, X.; O'Lenick, T. G.; Zhao, B. *Soft Matter* **2010**, *6*, 3325.

(8) Gutowska, A.; Jeong, B.; Jasionowski, M. *The Anatomical Record* **2001**, *263*, 342.

(9) Verber, R.; Blanazs, A.; Armes, S. *Soft Matter* **2012**, *8*, 9915.

(10) Zhang, L.; Eisenberg, A. *Science* **1995**, *268*, 23.

(11) Won, Y.-Y.; Davis, H. T.; Bates, F. S. *Science* **1999**, *283*, 960.

(12) Discher, D. E.; Eisenberg, A. *Science* **2002**, *297*, 967.

(13) Blanazs, A.; Madsen, J.; Battaglia, G.; Ryan, A. J.; Armes, S. P. *Journal of the American Chemical Society* **2011**, *133*, 16581.

(14) Blanazs, A.; Ryan, A. J.; Armes, S. P. *Macromolecules* **2012**, *45*, 5099.

(15) Gregory, C. D.; Milner, A. E. *International Journal of Cancer* **1994**, *57*, 419.

(16) Sonna, L. A.; Fujita, J.; Gaffin, S. L.; Lilly, C. M. *Journal of Applied Physiology* **2002**, *92*, 1725.
(17) Ohsaka, Y.; Ohgiya, S.; Hoshino, T.; Ishizaki, K. *Cellular Physiology and Biochemistry* **2002**, *12*, 111.
(18) Dresios, J.; Aschrafi, A.; Owens, G. C.; Vanderklish, P. W.; Edelman, G. M.; Mauro, V. P. *Proceedings of the National Academy of Sciences of the United States of America* **2005**, *102*, 1865.
(19) Al-Fageeh, M.; Smales, C. *Biochem. J* **2006**, *397*, 247.
(20) Neutelings, T.; Lambert, C. A.; Nusgens, B. V.; Colige, A. C. *PloS One* **2013**, *8*, e69687.
(21) Han, S.; Hagiwara, M.; Ishizone, T. *Macromolecules* **2003**, *36*, 8312.
(22) Lutz, J.-F.; Hoth, A. *Macromolecules* **2005**, *39*, 893.
(23) Ilavsky, J.; Jemian, P. R. *Journal of Applied Crystallography* **2009**, *42*, 347.
(24) Zhang, F.; Ilavsky, J.; Long, G. G.; Quintana, J. P. G.; Allen, A. J.; Jemian, P. R. *Metallurgical and Materials Transactions A-Physical Metallurgy and Materials Science* **2010**, *41A*, 1151.
(25) Lutz, J.-F.; Andrieu, J.; Üzgün, S.; Rudolph, C.; Agarwal, S. *Macromolecules* **2007**, *40*, 8540.
(26) Lutz, J.-F.; Weichenhan, K.; Akdemir, Ö.; Hoth, A. *Macromolecules* **2007**, *40*, 2503.
(27) Madsen, J.; Armes, S. P.; Bertal, K.; MacNeil, S.; Lewis, A. L. *Biomacromolecules* **2009**, *10*, 1875.
(28) Sun, S.; Wu, P. *Macromolecules* **2013**, *46*, 236.
(29) Pedersen, J. S. *Journal of Applied Crystallography* **2000**, *33*, 637.
(30) Pedersen, J. S.; Schurtenberger, P. *Macromolecules* **1996**, *29*, 7602.
(31) Pedersen, J. S.; Gerstenberg, M. C. *Colloids and Surfaces A-Physicochemical and Engineering Aspects* **2003**, *213*, 175.
(32) Hammouda, B.; National Institute of Standards and Technology: 2008.
(33) Kaya, H. *Journal of Applied Crystallography* **2004**, *37*, 223.
(34) Pedersen, J. S. *Journal of Chemical Physics* **2001**, *114*, 2839.
(35) Arleth, L.; Bergstrom, M.; Pedersen, J. S. *Langmuir* **2002**, *18*, 5343.
(36) Kinning, D. J.; Thomas, E. L. *Macromolecules* **1984**, *17*, 1712.
(37) Fetters, L. J.; Lohsey, D. J.; Colby, R. H. In *Physical Properties of Polymers Handbook*; 2nd ed.; Mark, J. E., Ed.; Springer: New York, 2007, p 447.
(38) Blanazs, A.; Armes, S. P.; Ryan, A. J. *Macromolecular Rapid Communications* **2009**, *30*, 267.
(39) Kocik, M.; Mykhaylyk, O.; Armes, S. *Soft Matter* **2014**.
(40) Fielding, L. A.; Lane, J. A.; Derry, M. J.; Mykhaylyk, O. O.; Armes, S. P. *Journal of the American Chemical Society* **2014**, *136*, 5790.

List of Tables

Table 1. DEGMA contents, conversions, molecular weights, polydispersities and CGT values obtained for $PGMA_{59}$-P($HPMA_x$-*stat*-$DEGMA_y$) statistical diblock copolymers and the corresponding $PGMA_{59}$ macro-CTA precursor (denoted as G_{59}). [For brevity, G = PGMA, H = PHPMA and D = PDEGMA].

Table 2. Structural parameters obtained from SAXS data fitting: volume fraction of the copolymer (ϕ), cross-section radius (R, nm) of worms (R_{sw}) or spheres (R_s) and its standard deviation (σ_R, nm), solvent volume fraction in the micelle core (x_{sol}), radius of gyration of the corona block (R_g, nm), contour length of the worms (L_w, nm), Kuhn length of the worms (b_w, nm), interaction radius of spheres (R_{PY}, nm) or characteristic length of worm-like micelles (L_c, nm) and the hard-sphere volume fraction of interacting sphere micelles (f_{PY}) or effective coefficient of worm-like micelle concentration (μ). If not specified in brackets, errors in the fitted parameters are within a unit of the last digit of the value.

Table 1. DEGMA contents, conversions, molecular weights, polydispersities and CGT values obtained for $PGMA_{59}$-P($HPMA_x$-*stat*-$DEGMA_y$) statistical diblock copolymers and the corresponding $PGMA_{59}$ macro-CTA precursor (denoted as G_{59}). [For brevity, G = GMA, H = HPMA and D = DEGMA].

Target Block Composition	DEGMA content[a] (mol %)	Conversion[b] (%)	M_n[c]	M_w/M_n[c]	CGT[d] (°C)
G_{59} macro-CTA	N/A	78	16,000	1.18	N/A
G_{59}-(H_{126}-D_{14})	10	98	40,200	1.11	23
G_{59}-(H_{135}-D_{15})	10	>99	40,800	1.11	20
G_{59}-(H_{144}-D_{16})	10	99	42,100	1.12	16
G_{59}-(H_{112}-D_{28})	20	>99	39,900	1.13	24
G_{59}-(H_{120}-D_{30})	20	>99	41,700	1.14	21
G_{59}-(H_{128}-D_{32})	20	>99	43,300	1.14	19
G_{59}-(H_{77}-D_{33})	30	>99	35,000	1.13	42
G_{59}-(H_{84}-D_{36})	30	97	37,000	1.14	34
G_{59}-(H_{91}-D_{39})	30	99	38,000	1.14	31
G_{59}-(H_{98}-D_{42})	30	>99	40,300	1.14	27
G_{59}-(H_{105}-D_{45})	30	98	40,400	1.15	25
G_{59}-(H_{112}-D_{48})	30	>99	44,000	1.15	21

a. Expressed as a proportion of the core-forming block
b. Monomer conversion determined by ^{1}H NMR spectroscopy
c. Determined by DMF GPC using poly(methyl methacrylate) calibration standards
d. Determined using a temperature sweep from low temperature to high temperature. The point at which G' intersects G'' is taken to be the CGT.

Table 2. Structural parameters obtained from SAXS data fitting: volume fraction of the copolymer (ϕ), cross-section radius (R, nm) of worms (R_{sw}) or spheres (R_s) and its standard deviation (σ_R, nm), solvent volume fraction in the micelle core (x_{sol}), radius of gyration of the corona block (R_g, nm), contour length of the worms (L_w, nm), Kuhn length of the worms (b_w, nm), interaction radius of spheres (R_{PY}, nm) or characteristic length of worm-like micelles (L_c, nm) and the hard-sphere volume fraction of interacting sphere micelles (f_{PY}) or effective coefficient of worm-like micelle concentration (μ). If not specified in brackets, errors in the fitted parameters are within a unit of the last digit of the value.

Morphology, conditions	ϕ	R	σ_R	x_{sol}	R_g	L_w	b_w	R_{PY} or L_c	f_{PY} or μ
Worms, original	0.036	8.7	1.1	0.35	1.8	102	10.0	-	-
Worms, original, PRISM structure factor included	*0.037*	*8.7*	*1.1*	*0.35*	*1.8*	*102*	*10.1*	*156*	*0.05*
Spheres, cooling	0.087	9.6	2.1	0.57	2.3	-	-	19.2(5)	0.053(3)
Spheres, cooling, corona profile function used	*0.091*	*9.6*	*2.0*	*0.60*	*2.3*	-	-	*20.5(2)*	*0.048(2)*
Spheres, heating	0.086	9.7	2.1	0.55	2.4	-	-	20.6(8)	0.044(3)
Worms, heating	0.036	8.7	1.1	0.35	1.8	100	9.7	-	-

List of Schemes

Scheme 1. (a) Synthesis of thermo-responsive $PGMA_{59}$-P($HPMA_x$-*stat*-$DEGMA_y$) diblock copolymers prepared via RAFT aqueous dispersion polymerization. The precise values of x and y dictate the critical gelation temperature (CGT) observed for the worm gel phase. (b) Schematic representation of the reversible worm-to-sphere-to-unimer thermal transitions.

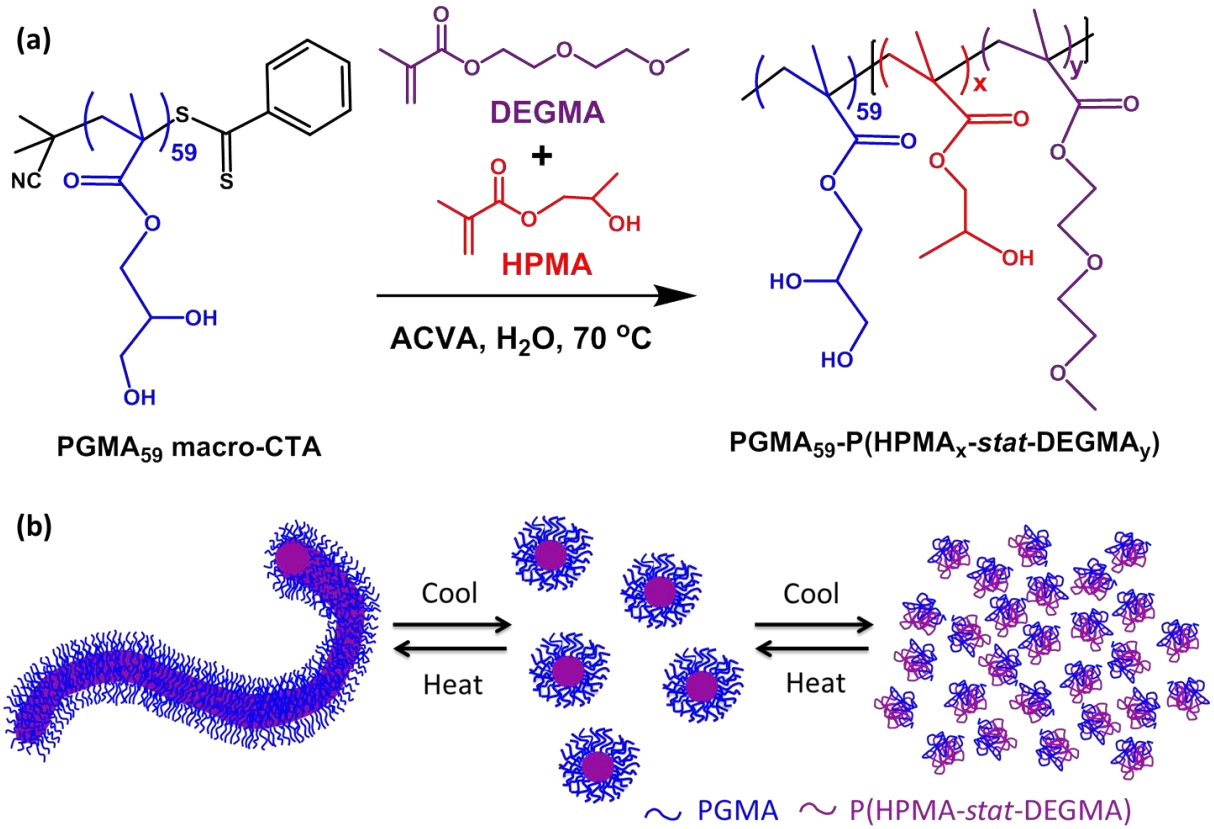

Scheme 1. (a) Synthesis of thermo-responsive $PGMA_{59}$-$P(HPMA_x$-*stat*-$DEGMA_y)$ diblock copolymers prepared via RAFT aqueous dispersion polymerization. The precise values of x and y dictate the critical gelation temperature (CGT) observed for the worm gel phase. (b) Schematic representation of the reversible worm-to-sphere-to-unimer thermal transitions.

List of Figures

Figure 1. DMF GPC curves recorded for: (a) $PGMA_{59}$ and $PGMA_{59}$-P($HPMA_x$-*stat*-$DEGMA_y$) copolymers prepared with 10 mol % DEGMA in the core-forming block; (b) $PGMA_{59}$ and $PGMA_{59}$-P(HPMA-*stat*-$DEGMA)_{140}$ copolymers comprising varying DEGMA content of the core-forming block (where G = GMA, H = HPMA and D = DEGMA).

Figure 2. (a) Temperature dependence of the storage (G') and loss (G'') moduli for $PGMA_{59}$-P($HPMA_{144}$-*stat*-$DEGMA_{16}$) and $PGMA_{59}$-P($HPMA_{126}$-*stat*-$DEGMA_{14}$), both prepared with 10 mol% DEGMA in the core-forming block. On heating from 10 to 40°C, the G' and G'' curves cross over at a critical gelation temperature (CGT) of either 16°C or 23°C. (b) Relationship between CGT and the overall DP of the core-forming block for $PGMA_{59}$-P(HPMA-*stat*-$DEGMA)_x$ statistical diblock copolymers, where x = 140, 150 and 160 for the 10, 20 and 30 mol% DEGMA contents, respectively. Conditions: frequency = 1.0 rad s^{-1} at an applied strain of 1.0%.

Figure 3. Variation of the critical gelation temperature (CGT) with overall DP of the core-forming block (x) for $PGMA_{59}$-P(HPMA-*stat*-$DEGMA)_x$ prepared using 30 mol% DEGMA (where x = 110, 120, 130, 140, 150 or 160). Inset: digital images of $PGMA_{59}$-P($HPMA_{91}$-*stat*-$DEGMA_{39}$). A clear free-flowing liquid is obtained below the CGT of 31°C, whereas a transparent free-standing gel is formed above this CGT.

Figure 4. TEM images obtained for G_{59}-(H_x-*stat*-D_y) prepared with 10, 20 or 30 mol% DEGMA in the core-forming statistical block (where G, H and D denote GMA, HPMA and DEGMA, respectively).

Figure 5. Visible absorption spectra recorded for: (a) a series of $PGMA_{59}$-P(HPMA-*stat*-$DEGMA)_{160}$ prepared using 10, 20 or 30 mol% DEGMA, (b) a series of $PGMA_{59}$-P(HPMA-*stat*-$DEGMA)_x$ diblock copolymers prepared using 30 mol% DEGMA while varying the core-forming block DP (where x = 140, 150, 160), (c) a 10% w/w aqueous dispersion of $PGMA_{59}$-P($HPMA_{91}$-*stat*-$DEGMA_{39}$) showing the change in turbidity observed during a 40°C-25°C-5°C-25°C-40°C thermal cycle. The reduction in absorbance on cooling is the result of a worm-to-sphere transition occurring at around 31°C, since the worms scatter visible light more effectively than the smaller spheres (especially at shorter λ). A further significant reduction in turbidity occurs at 5°C, which is consistent with molecular dissolution of the copolymer chains (see Scheme 1b). The almost perfect overlay of spectra recorded during the cooling and heating cycles suggest that these thermally-induced order-order and order-disorder morphological transitions have good reversibility.

Figure 6. ^1H NMR spectra (D_2O) recorded for a 10% w/w copolymer dispersion of $PGMA_{59}$-P($HPMA_{91}$-*stat*-$DEGMA_{39}$) from 5 to 40°C. Disappearance of the two pendent methyl signals assigned to DEGMA (m) and HPMA (h) is indicated by the vertical dotted lines. Sodium 2,2-dimethyl 2-silapentane-5-sulfonate (DSS) was used as an internal standard.

Figure 7. Time-resolved SAXS patterns recorded for a 4.8% w/w aqueous dispersion of $PGMA_{59}$-P($HPMA_{91}$-*stat*-$DEGMA_{39}$) during cooling from 40°C to 5°C at 1°C min^{-1}. The solid red line indicates the reduction in SAXS intensity at low q during cooling.

Figure 8. Selected SAXS patterns recorded for a 4.8% w/w aqueous dispersion of $PGMA_{59}$-P($HPMA_{91}$-*stat*-$DEGMA_{39}$) at 40°C, 25°C, 20°C, 15°C and 5°C during cooling (circles) and subsequent heating (triangles). The solid lines represent fits to the cooling data using the worm-like micelle model (at 40°C), a spherical micelle model (at 20°C) and a generalized Gaussian coil model for molecularly-dissolved copolymer chains (at 5°C). The inset shows the Porod-invariant $Q = \int_{q_{min}}^{q_{max}} \frac{d\Sigma}{d\Omega}(q) q^2 dq$ calculated from experimental SAXS patterns (q_{min} = 0.016 nm^{-1} and q_{max} = 1.6 nm^{-1}) recorded during the cooling and heating cycles.

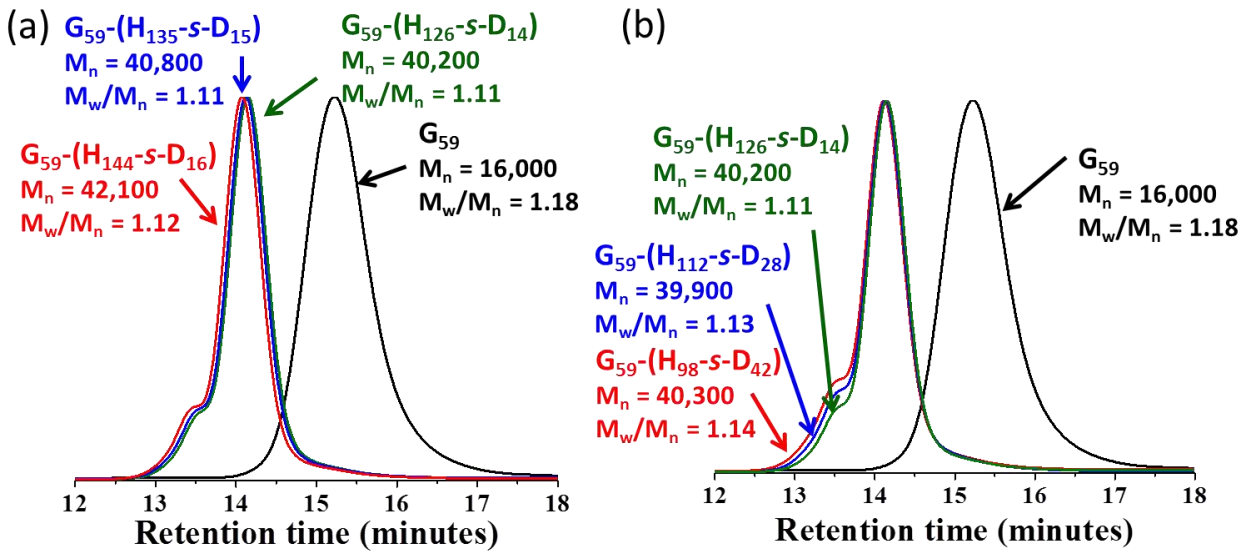

Figure 1. DMF GPC curves recorded for: (a) $PGMA_{59}$ and $PGMA_{59}$-P($HPMA_x$-*stat*-$DEGMA_y$) copolymers prepared with 10 mol % DEGMA in the core-forming block; (b) $PGMA_{59}$ and $PGMA_{59}$-P(HPMA-*stat*-$DEGMA)_{140}$ copolymers comprising varying DEGMA content of the core-forming block (where G = GMA, H = HPMA and D = DEGMA).

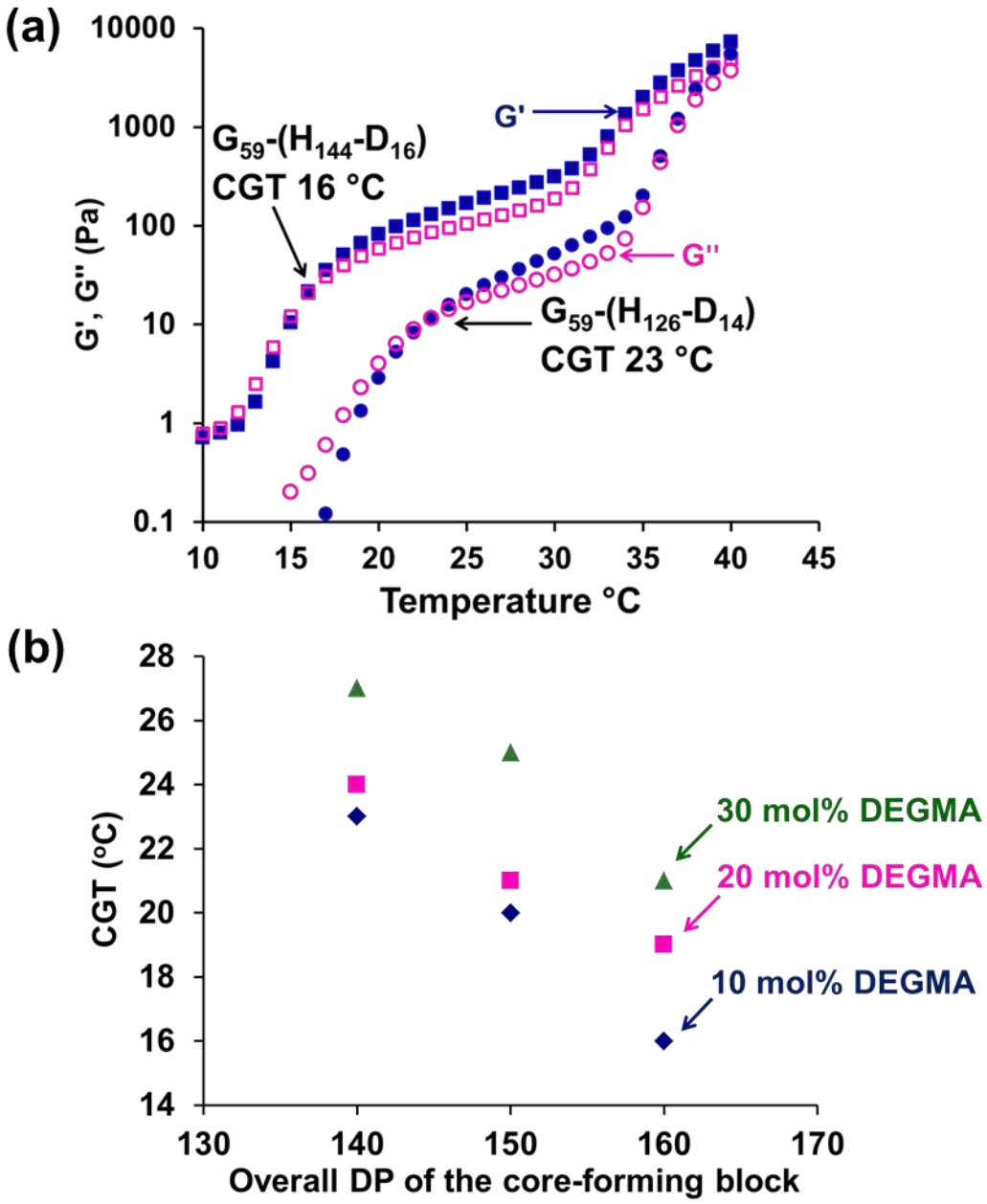

Figure 2. (a) Temperature dependence of the storage (G') and loss (G'') moduli for $PGMA_{59}$-P($HPMA_{144}$-*stat*-$DEGMA_{16}$) and $PGMA_{59}$-P($HPMA_{126}$-*stat*-$DEGMA_{14}$), both prepared with 10 mol% DEGMA in the core-forming block. On heating from 10 to 40°C, the G' and G'' curves cross over at a critical gelation temperature (CGT) of either 16°C or 23°C. (b) Relationship between CGT and the overall DP of the core-forming block for $PGMA_{59}$-P(HPMA-*stat*-$DEGMA)_x$ statistical diblock copolymers, where x = 140, 150 and 160 for the 10, 20 and 30 mol% DEGMA contents, respectively. Conditions: frequency = 1.0 rad s^{-1} at an applied strain of 1.0%.

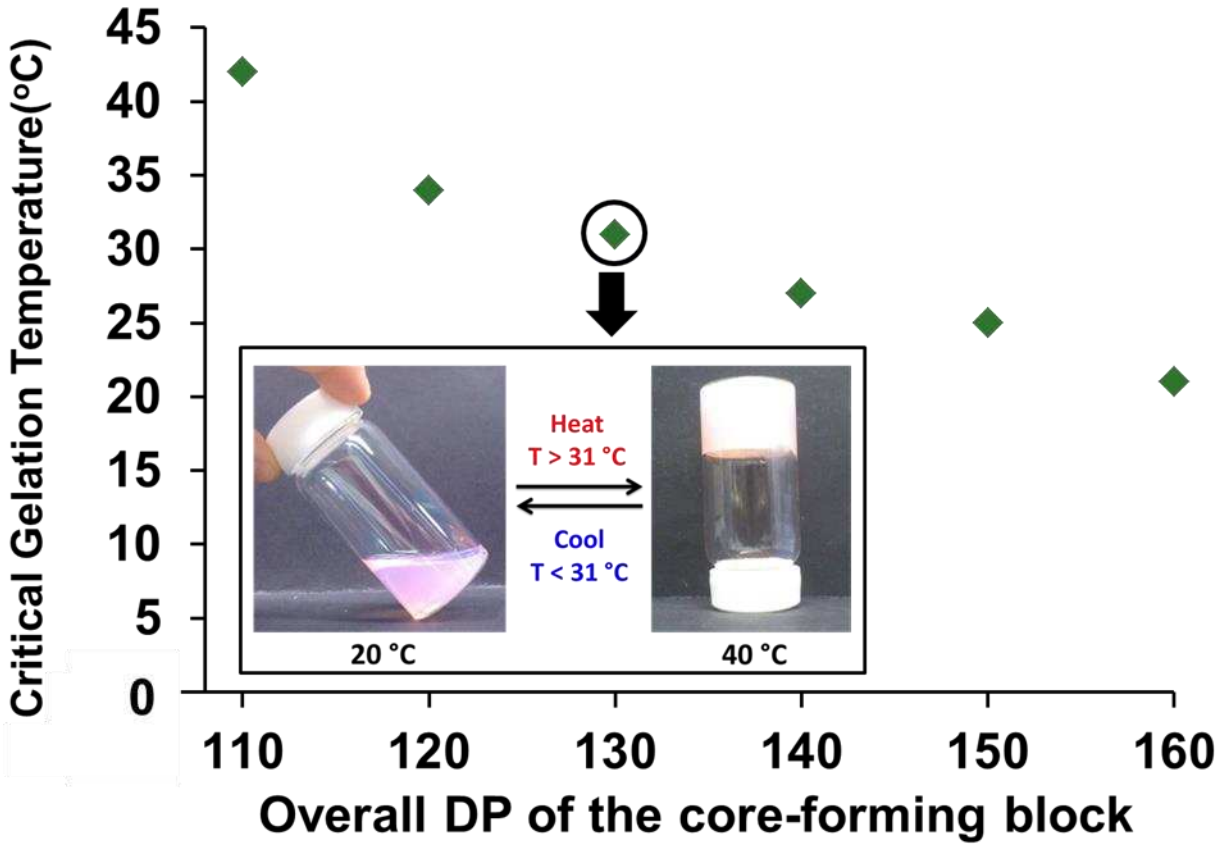

Figure 3. Variation of the critical gelation temperature (CGT) with overall DP of the core-forming block (x) for $PGMA_{59}$-P(HPMA-*stat*-DEGMA)$_x$ prepared using 30 mol% DEGMA (where x = 110, 120, 130, 140, 150 or 160). Inset: digital images of $PGMA_{59}$-$P(HPMA_{91}$-*stat*-$DEGMA_{39})$. A clear free-flowing liquid is obtained below the CGT of 31°C, whereas a transparent free-standing gel is formed above this CGT.

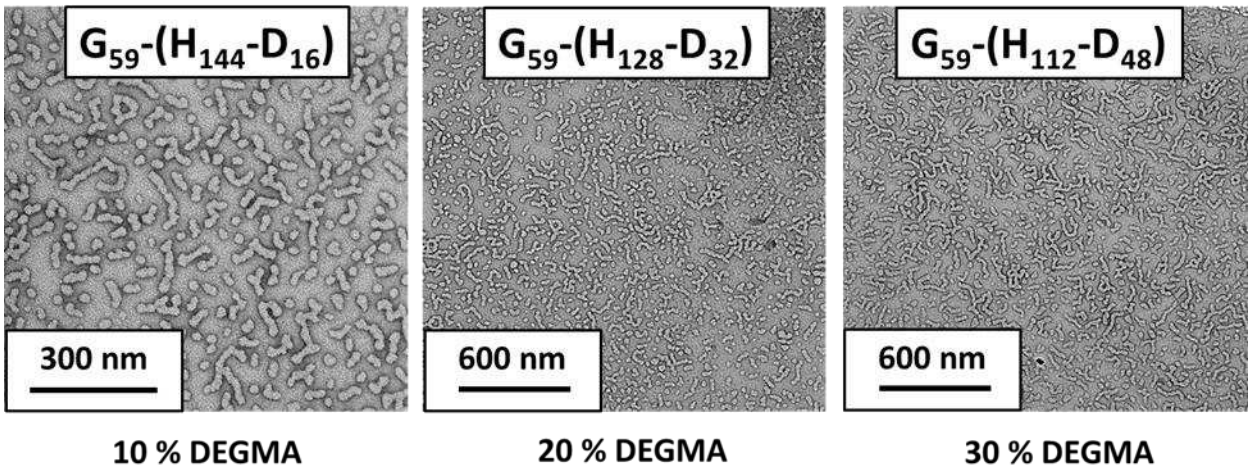

Figure 4. TEM images obtained for G_{59}-(H_x-*stat*-D_y) prepared with 10, 20 or 30 mol% DEGMA in the core-forming statistical block (where G, H and D denote GMA, HPMA and DEGMA, respectively).

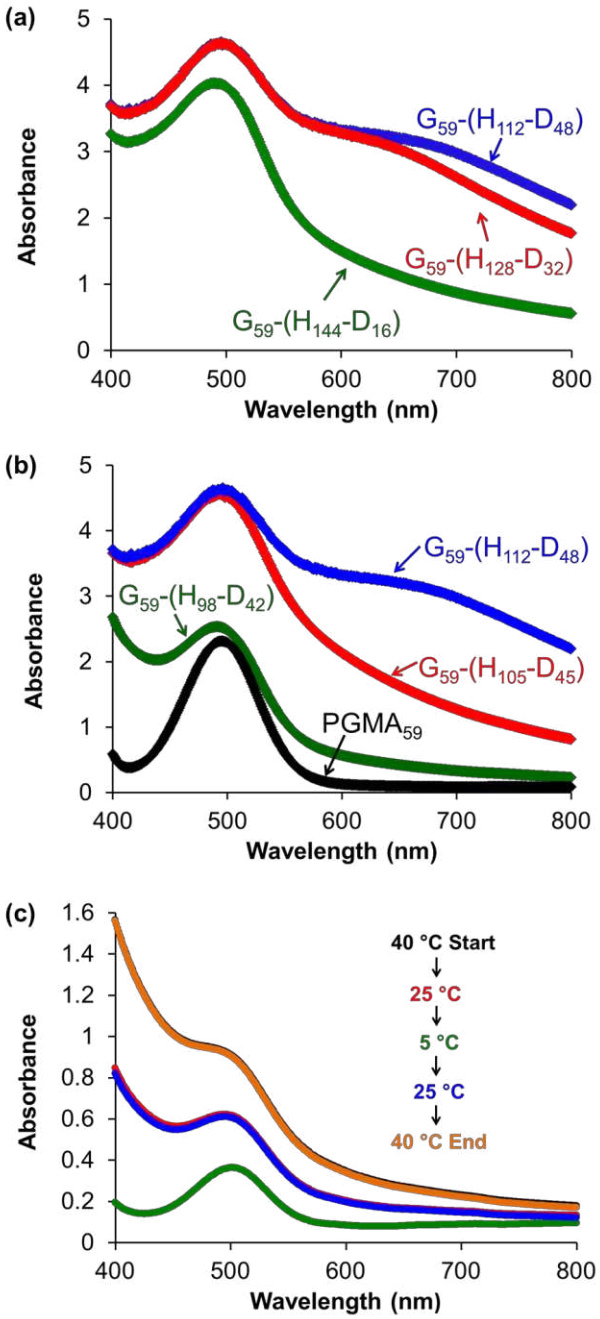

Figure 5. Visible absorption spectra recorded for: (a) a series of $PGMA_{59}$-P(HPMA-*stat*-$DEGMA)_{160}$ prepared using 10, 20 or 30 mol% DEGMA, (b) a series of $PGMA_{59}$-P(HPMA-*stat*-$DEGMA)_x$ diblock copolymers prepared using 30 mol% DEGMA while varying the core-forming block DP (where x = 140, 150, 160), (c) a 10% w/w aqueous dispersion of $PGMA_{59}$-P($HPMA_{91}$-*stat*-$DEGMA_{39}$) showing the change in turbidity observed during a 40°C-25°C-5°C-25°C-40°C thermal cycle. The reduction in absorbance on cooling is the result of a worm-to-sphere transition occurring at around 31°C, since the worms scatter visible light more effectively than the smaller spheres (especially at shorter λ). A further significant reduction in turbidity occurs at 5°C, which is consistent with molecular dissolution of the copolymer chains (see Scheme 1b). The almost perfect overlay of spectra recorded during the cooling and heating cycles suggest that these thermally-induced order-order and order-disorder morphological transitions have good reversibility.

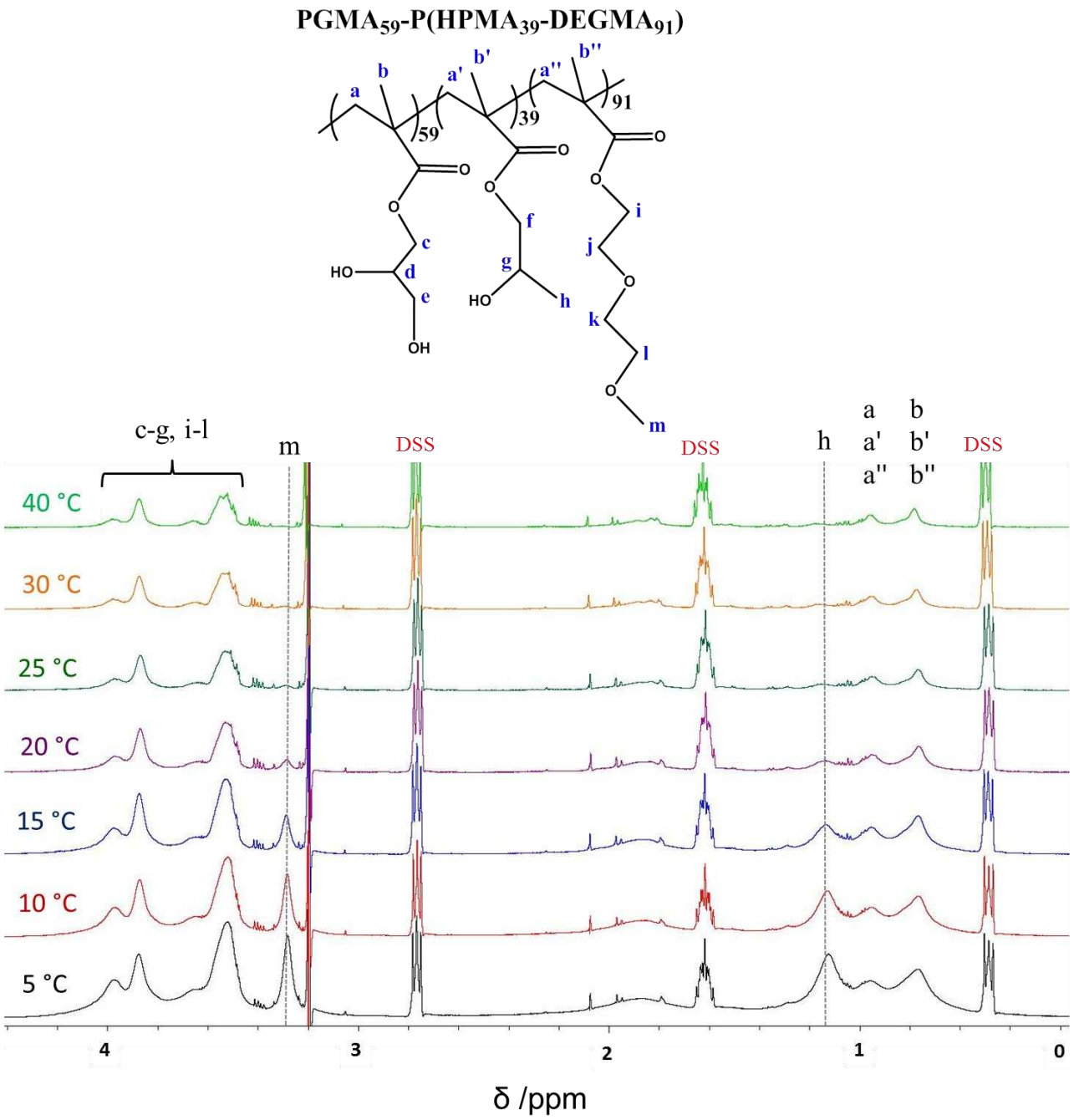

Figure 6. ^{1}H NMR spectra (D_2O) recorded for a 10% w/w copolymer dispersion of $PGMA_{59}$-P($HPMA_{91}$-*stat*-$DEGMA_{39}$) from 5 to 40°C. Disappearance of the two pendent methyl signals assigned to DEGMA (m) and HPMA (h) is indicated by the vertical dotted lines. Sodium 2,2-dimethyl 2-silapentane-5-sulfonate (DSS) was used as an internal standard.

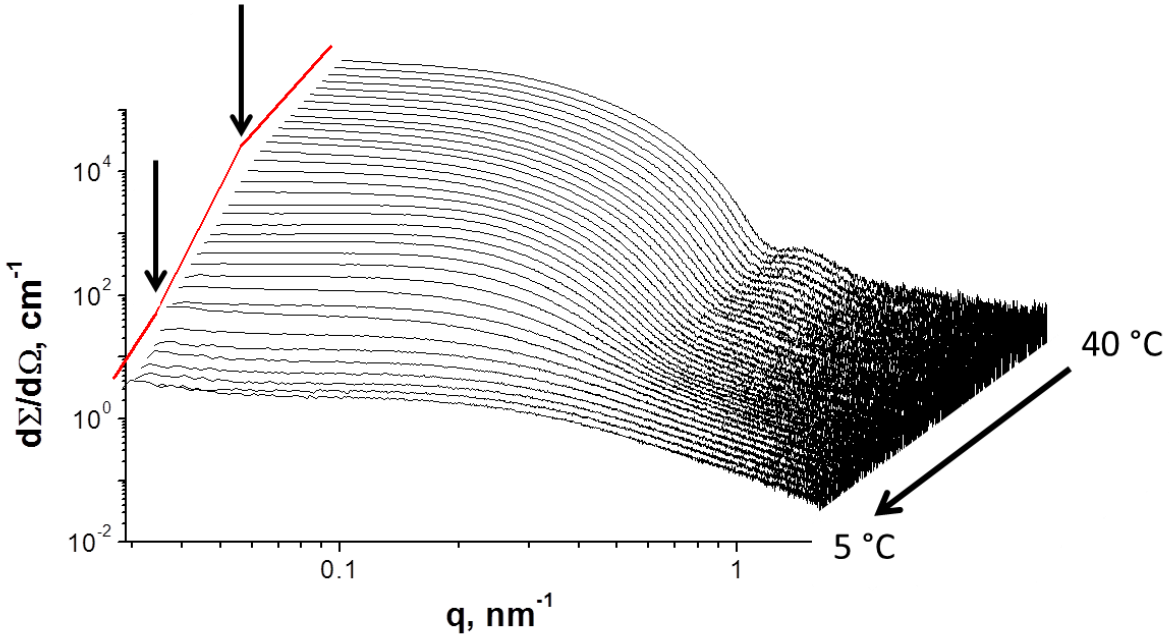

Figure 7. Time-resolved SAXS patterns recorded for a 4.8% w/w aqueous dispersion of $PGMA_{59}$-P($HPMA_{91}$-*stat*-$DEGMA_{39}$) during cooling from 40°C to 5°C at 1°C min^{-1}. The solid red line indicates the reduction in SAXS intensity at low *q* during cooling.

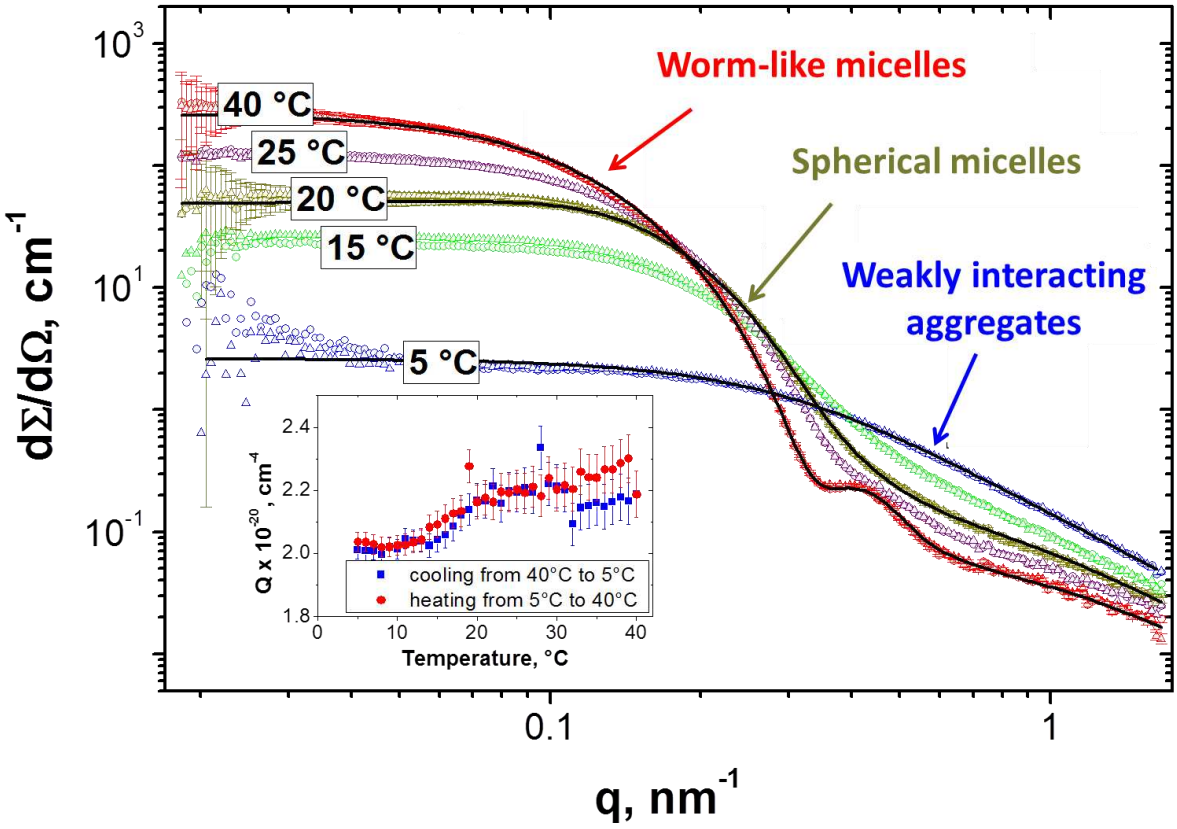

Figure 8. Selected SAXS patterns recorded for a 4.8% w/w aqueous dispersion of $PGMA_{59}$-P($HPMA_{91}$-*stat*-$DEGMA_{39}$) at 40°C, 25°C, 20°C, 15°C and 5°C during cooling (circles) and subsequent heating (triangles). The solid lines represent fits to the cooling data using the worm-like micelle model (at 40°C), a spherical micelle model (at 20°C) and a generalized Gaussian coil model for molecularly-dissolved copolymer chains (at 5°C). The inset shows the Porod-invariant $Q = \int_{q_{min}}^{q_{max}} \frac{d\Sigma}{d\Omega}(q) q^2 dq$ calculated from experimental SAXS patterns (q_{min} = 0.016 nm^{-1} and q_{max} = 1.6 nm^{-1}) recorded during the cooling and heating cycles.